REFERENCES

1. Speciale, R. A., "A Generalization of the TSD Network Analyzer Calibration Procedure Covering n-port Scattering Parameter Measurements Affected by Leakage Errors," IEEE Trans. on Microwave Theory and Techniques, vol. MTT-25, pp 1100-1115, December 1977.

2. Mondal, J. P. and Chen, T. H., "Propagation Constant Determination in Microwave Fixture Deembedding Procedure," IEEE Trans. on Microwave Theory and Techniques, vol. MTT-36, no. 4, pp 706-714, April 1988.

3. Lang, R. J., Jewett, W., and Merrill, J., "Test Fixtures for Frequencies From DC to 75 GHz", Microwave Journal, May 1988.

International Journal of Infrared and Millimeter Waves, Vol. 10, No. 6, 1989

MPM—AN ATMOSPHERIC MILLIMETER-WAVE PROPAGATION MODEL

Hans J. Liebe

National Telecommunications and Information Administration,
Institute for Telecommunication Sciences,
325 Broadway
Boulder, Colorado 80303

Received February 1, 1989

A broadband model for complex refractivity is presented to predict propagation effects of loss and delay for the neutral atmosphere at frequencies up to 1000 GHz. Contributions from dry air, water vapor, suspended water droplets (haze, fog, cloud), and rain are addressed. For clear air, the local line base (44 O_2 plus 30 H_2O lines) is complemented by an empirical water-vapor continuum. Input variables are barometric pressure, temperature, relative humidity, suspended water droplet concentration, and rainfall rate.

Key Words: Atmospheric propagation model; specific attenuation and phase dispersion; complex refractivity; microwave to submillimeter-wavelengths.

1. INTRODUCTION

The parameters of a radio wave are modified on propagation through the neutral atmosphere. In general, such influences are due to refraction, absorption, and scatter. The complex refractive index,

$$n = n' - jn'',$$

0195-9271/89/0600-0631$06.00/0

is a measure of the interaction of electromagnetic radiation with the atmospheric medium. Both phase and amplitude responses of a plane radio wave propagating the distance L at frequency f follow from

$$E(L) = E_o \exp[-j(2\pi f/c)L \cdot n],$$

where E_o is the initial amplitude, c is the speed of light in vacuum, and $j = \sqrt{-1}$. The index n depends on frequency and atmospheric conditions. Its real part exceeds unity by a small amount ($n' - 1 \leq 0.0005$) slowing the propagation velocity to values less than c, while the associated positive imaginary part ($n'' \leq 0.001$) reduces the amplitude E_o.

Complex refractivity, defined in units of parts per million as

$$N = (n - 1)10^6 \quad \text{ppm}, \qquad (1)$$

is introduced as a practical measure to characterize conveniently the refractive index of the atmosphere. A physical model of refractivity N is discussed here for atmospheric conditions affecting frequencies up to 1000 GHz.

1.1. Features of the MPM Code

The concept of an atmospheric millimeter-wave propagation model (the MPM) in the form of $N(f)$ had been introduced in [1]. Modular, quantitative relationships were developed between meteorological conditions encountered in the neutral atmosphere and corresponding refractivity formulations. In this paper the contributions by dry air, water vapor, and suspended water droplets (haze, fog, cloud) are reviewed and revised. A single-parameter approximation for rain effects is added. For readers interested in a detailed exposition of the microphysical formulations underlying gaseous millimeter-wave absorption, the excellent summary in [2] is recommended.

Refractivity of moist air can be obtained, in principle, by considering all known resonant, far-wing, and nonresonant radio-wave interactions with the gaseous molecules which are in a given volume element. For example, the number of contributing spectral lines by the major absorber H_2O exceeds 1000, located below and above 1 THz; in addition, not all interaction processes are well understood. To model $N(f)$, various degrees of approximations have been employed to reduce labor and computer time, as well as to bridge unknowns. The MPM consists of 44 O_2 and 30 H_2O local (below 1000 GHz) line spectra and an empirical water vapor term which reconciles discrepancies with observed absorptions; further, nonresonant spectra of dry air and refractivity formulations for suspended water droplets (simulating haze, fog, or cloud conditions) and rain are added to complete the model.

Input variables of MPM are frequency ($f \leq 1000$ GHz) and the atmospheric parameters identified below:

Input	Symbol	Validity Range	Medium
barometric pressure.....	P	120 - 10^{-5} kPa	Moist
temperature.....	T	-50 - 50 °C	Air
relative humidity.....	U	0 - 100 %RH	
hygroscopic aerosol reference concentration.. growing for 80 to 99.9 %RH into suspended droplets	w_o(80 %RH)	0 - 1 mg/m^3,	Haze
suspended water droplet concentration.....	W(100 %RH)	0 - 5 g/m^3	Fog, Cloud
rainfall rate.....	R	0 - 200 mm/h	Rain

Spatial and temporal distributions of (P,T,U; W; R) along a radio path determine the absorber content and thereby the propagation characteristics of the path.

The mesospheric height range 30 to 100 km is dealt with approximately excluding the geomagnetic O_2-Zeeman effect and trace gas spectra (e.g., O_3, CO, N_2O, ClO, etc.). A complete Zeeman model for O_2 lines in the 60 GHz band and at 119 GHz was developed separately to analyze anisotropic propagation of polarized radio waves about ± 5 megahertz the line centers [3]. Ionospheric effects decrease above 1 GHz with the inverse square of frequency and become quickly ($f \geq 3$ GHz) negligible.

In the following section, a brief description of the atmospheric environment considered by MPM is presented and the relationships between input parameters and internal model variables are worked out.

1.2. Atmospheric Conditions: Input and Model Variables

Air conditions are measured by barometric pressure

$$P = p + e \quad \text{kPa},$$

where p and e are partial pressures for dry air and water vapor, respectively;
by temperature T in °C which is converted into a relative inverse temperature variable

$$\theta = 300/(T + 273.15);$$

and by relative humidity,

$$U = (e/e_S)100 \leq 100 \quad \%RH.$$

The temperature dependence of water vapor saturation pressure e_S (100 %RH) is approximated (error ≤ 0.2% over ± 40°C) and, in turn, expressed as vapor concentration,

$$v = 7.223e\theta = 1.739 \cdot 10^{9} U\theta^{5}\exp(-22.64\theta) \quad g/m^3. \qquad (2)$$

Equation (2) allows to correlate absolute (either concentration v or pressure e) and relative humidity U when the temperature T is known.

Typical weather conditions at sea level, assuming P = 101 kPa and T = 22°C (θ = 1.0164), encompass

	Dry	Normal	Humid	Saturated
U, %RH	5	50	85	100
v, g/m³	1	10	17	20
e, kPa	0.14	1.36	2.32	2.72 ,

and can vary considerably with time and location.

Hygroscopic aerosol is an atmospheric ingredient active with relative humidity. Solution droplets appear for U > 80 %RH, and haze conditions develop as saturation is approached. The growing haze droplets can reach concentrations (≤ 0.1 g/m³) that contribute to wave absorption. Haze conditions are modeled by assuming that for a given air mass (ID = A, B, C, D), the hygroscopic aerosol concentration w_o at a reference value U = 80 %RH is known. Swelling/shrinking to a droplet concentration W_A follows relative humidity variations over the range 80 to ≤ 99.9 %RH and is modeled by

$$W_A(RH) = w_o 10^{-3} g(U), \qquad (3)$$

where $g(U) = [20(C_1 + 4) - U]/C_1(100 - U)$

is a growth function. The parameter C_1 was inferred from results reported in [5] for four classes of air mass:

ID	Aerosol Species	C_1	g(99.9 %RH)
A	Rural	1.87	94
B	Urban	2.41	117
C	Maritime	5.31	163
D	C + Strong Wind (≥10 km/h)	5.83	166 .

Average values of w_o for different climatic situations can be found in the literature and may lie between 0.01 and 0.5 mg/m³. The humidity-dependent growth can be substantial as indicated by the maximum prefog value g(99.9 %RH).

Suspended hydrometeors representing fog/cloud conditions at 100 %RH are described by a water droplet concentration W, which can be deduced from measured drop size spectra or estimated as path-average from optical (0.55 μm) visibility data *VS*(km). Cloud coverage is a frequent event that typically occurs half of the time with vertical extensions of up to 2 km. A schematic description of droplet concentration and visibility can be made:

	Haze	Fog	Stratus..	Convective Cloud	
W ≤	0.01	0.1	1	5	g/m³
VS ≥	1.1	0.27	0.07	0.03	km .

Rain originates as a statistical event out of convective clouds suspended in saturated air. Its vertical distribution is separated into two regions by the height of the 0°C isotherm, which can vary between 6 km and ground level depending on season and latitude. The lower part is filled with liquid drops, and the upper region consists of frozen particles with occasional supercooled drop-loadings by strong updrafts.

Point rainfall rates, R, have proven useful in modeling propagation effects due to rain and such rates are related:

- to percent time (t_R) a value occurs over the period of an average year;
- to an effective rain cell extent L_R/L; and
- to the momentarily suspended liquid water concentration,

$$W_R = m_R \cdot R \quad g/m^3.$$

In terms of these quantities, typical mid-latitude rain may be classified as follows (horizontal path, L = 10 km):

	Drizzle	Steady	Heavy	Downpour	Cloudburst	
R	1	5	20	100	200	mm/h
t_R	2	0.5	0.07	0.001	0.0001	%/yr
L_R/L	1	1	0.7	0.35	0.2	
m_R	0.1	0.07	0.05	0.04	0.04	

The simple coefficient scheme reveals some fundamentals of rain. Changes in the factor m_R indicate rain-rate dependent characteristics of drop size distributions. Widespread steady rain occurs more uniformly and favors small drop sizes ($\leq$ 1 mm diameter) which stay longer in the air. Heavy showers are more localized, favor larger drops ($\leq$ 5 mm diameter) and occur less frequently.

In summary, six meteorological input parameters (i.e., P,T,U; w_o,W; R) have been characterized for MPM and correlated to model-specific physical variables (p, e, v, θ, W_A).

2. COMPLEX REFRACTIVITY MODEL

Atmospheric refractivity characteristics are assessed from known meteorological variables. A parametric program was developed to calculate complex dispersive refractivity,

$$N_t(f) = N_o + N(f) = N_o + N'(f) - jN''(f) \quad \text{ppm}, \qquad (4)$$

where the nondispersive part N_o is real and positive and N is a function of frequency. Refractivity is easily converted into path-specific propagation rates; i.e., the imaginary part of (4) leads to power attenuation

$$\alpha = 0.1820f\ N''(f) \quad \text{dB/km}, \qquad (5a)$$

and the real part to phase dispersion

$$\beta = 1.2008f\ N'(f) \quad \text{deg/km},$$

or group delay

$$\tau = 3.336\ N'(f) \quad \text{ps/km}, \qquad (5b)$$

where frequency f is in gigahertz (GHz) throughout.

Nondispersive refractivity is expressed by the sum of four contributions,

$$N_o = (N_1 + N_2) + N_3 + N_4 , \qquad (6)$$

which relate to meteorological parameters as follows,

$N_1 = 2.588p\theta$ ... dry air,
$N_2 = (41.63\theta + 2.39)e\theta$ ... water vapor,

$N_3 = W\ (3/2)[1 - 3/(\epsilon_o + 2)]$ ... susp. droplets,
$N_4 \approx R(3.7 - 0.012R)/k_R$ ... rain.

Results for $N_{1,2}$ are from microwave experiments at frequencies where dispersive contributions $N'(f)$ are negligible. Formulations for $N_{3,4}$ are derived from analytical models [see (16), also for ϵ_o; and (18), also for k_R].

Dispersive complex refractivity is defined N = 0 at f = 0 and can be represented by five terms,

$$N = (N_L + N_d + N_c) + N_W + N_R , \qquad (7)$$

identifying

- N_L - moist air resonance contributions (i = 48 oxygen and k = 30 water vapor lines),
  N_d - dry air nonresonant spectra,
  N_c - water vapor continuum spectrum;
- N_W - suspended water-droplet refractivity;
- N_R - rain approximation;

which are discussed in detail in sections 2.1. to 2.5.

2.1. Local Line Absorption and Dispersion

A line-by-line summation of spectra by the two principle absorber molecules, O_2 and H_2O, yields the resonance contribution,

$$N_L = \sum_{i=1}^{44} S_i F(f)_i + \sum_{k=1}^{30} S_k F(f)_k , \qquad (8)$$

where S is a line strength in kHz, $F = F' - jF''$ is a complex shape function in GHz^{-1}, and i,k are the line indices. The Van Vleck-Weisskopf shape function was used as modified by Rosenkranz [6] to describe pressure-induced line interference. Line spectra of absorption (F") and dispersive refractivity (F') take the form

$$F''(f) = A/X + A/Y - \delta(f/\nu_o)[(\nu_o - f)/X + (\nu_o + f)/Y],$$
and
$$F'(f) = (B-f)/X + (B+f)/Y - 2/\nu_o + \delta(A/X - A/Y), \qquad (9)$$

with the abbreviations

$$A = \gamma f/\nu_o, \qquad B = (\nu_o^2+\gamma^2)/\nu_o \approx \nu_o,$$
$$X = (\nu_o - f)^2 + \gamma^2, \qquad Y = (\nu_o + f)^2 + \gamma^2.$$

The line parameters are:

Symbol	O_2 Lines in Air (i)	H_2O Lines in Air (k)	
S, kHz	$a_1 10^{-6} p\theta^3 \exp[a_2(1-\theta)]$	$b_1 e\theta^{3.5} \exp[b_2(1-\theta)]$	(10)
γ, GHz	$a_3 10^{-3}(p\theta^{(0.8-a4)} + 1.1e\theta)$	$b_3 10^{-3}(p\theta^{b4} + b_5 e\theta^{b6})$	(11)
δ	$(a_5 + a_6\theta)10^{-3} p\theta^{0.8}$	0	(12)

Line center frequencies ν_o in GHz and the spectroscopic parameters a_{1-6} and b_{1-6} for strength S, pressure-broadened width γ, and pressure-induced interference δ are listed in TABLE 1. A strength cutoff of $S_i/p = 10^{-6}$ (O_2) and $S_k/e = 10^{-3}$ kHz/kPa (H_2O) was applied ($\theta = 1$). Entries in TABLE 1 for $\nu_o(O_2)$ [7], a_2, b_2 and $a_{5,6}$ [2], and b_3 to b_6 [8] were revised or added when compared with the version in [1].

In view of stated uncertainties of about ± 10 percent for the theoretical line strength parameters b_1, it is acceptable to improve the computing efficiency of MPM by approximating the temperature dependence of the width parameters $b_{3,5}$ by setting $b_4 \approx 0.7$ and $b_6 \approx 0.9$.

Zeeman splitting of O_2 lines must be taken into account when extending height levels above 35 km [3]. A rough estimate of oxygen line behavior in the mesosphere can be made by keeping (9) and replacing the width γ_i (11) with

$$\gamma_i^h = (\gamma_i^2 + 625 \cdot B_o^2)^{\frac{1}{2}} \quad \text{GHz}, \qquad (11a)$$

where B_o is the geomagnetic field strength, ranging from (25 to 65)10^{-6} tesla depending on geographic location and altitude. The O_2 line spectrum vanishes above 100 km height.

At altitudes higher than 60 km ($P \leq 0.07$ kPa), Doppler-broadening has to be considered. The transition from pressure-broadening to Doppler-broadening is correctly modeled with a Voigt shape function. For MPM, weak H_2O lines in the mesosphere (mixing ratios lie between 3.5 and 5 ppmv over the altitude range 20 - 70 km) are approximated by retaining the shape function (9) and substituting the width γ_k (11) with

$$\gamma_k^h = 0.535\gamma_k + (0.217\gamma_k^2 + \gamma_D^2)^{\frac{1}{2}} \quad \text{GHz}, \qquad (11b)$$

where $\gamma_D^2 = 2.13 \cdot 10^{-12} \nu_o^2/\theta$ is the squared Doppler width.

Predicting H_2O-line attenuation under tropospheric conditions by means of (5a),(8),(9) to a level of significance of about ± 0.01 dB/km presents a serious test of the shape function $F_k''(f)$. Peak rates $\alpha_L(\nu_o) = 0.182\nu_o S/\gamma$ reach 10^5 dB/km for the strongest MPM line (ν_o= 557 GHz) and exceed 10^6 dB/km for H_2O lines above 1 THz. Any shape function expected to track eight orders of magnitude is probably overtaxed. The function F" is well behaved within the frequency range of line dominance where $[\alpha(f)/\alpha(\nu_o)]_L \geq 10^{-4}$, and when $f \to 0$; however, it predicts a finite non-zero value as $f \to \infty$ [4]. No line shape has been confirmed which is capable of predicting absorption intensities over ranges 10^{-3} to 10^{-8} the value at line center. Discrepancies between predicted and observed attenuations are accounted for summarily by an empirical correction (see Sect. 2.3.).

2.2. Nonresonant Dry Air Spectrum

Nonresonant refractivity terms of dry air make a small contribution at ground level pressures due to the Debye spectrum of oxygen below 10 GHz and pressure-induced nitrogen absorption that becomes effective above 100 GHz. The functional form is [1]

$$N_d''(f) = S_d f/\gamma_o[1+(f/\gamma_o)^2] + a_p f p^2 \theta^{3.5}$$
and
$$N_d'(f) = S_d(1/[1+(f/\gamma_o)^2] - 1), \qquad (13)$$

TABLE 1. Local Line Data Files Of MPM For Moist Air
(a_i for O_2, b_k for H_2O)

v0	a1	a2	a3	a4	a5	a6
50.474238	0.94	9.694	8.60	0	1.600	5.520
50.987749	2.46	8.694	8.70	0	1.400	5.520
51.503350	6.08	7.744	8.90	0	1.165	5.520
52.021410	14.14	6.844	9.20	0	0.883	5.520
52.542394	31.02	6.004	9.40	0	0.579	5.520
53.066907	64.10	5.224	9.70	0	0.252	5.520
53.595749	124.70	4.484	10.00	0	-0.066	5.520
54.130000	228.00	3.814	10.20	0	-0.314	5.520
54.671159	391.80	3.194	10.50	0	-0.706	5.520
55.221367	631.60	2.624	10.79	0	-1.151	5.514
55.783802	953.50	2.119	11.10	0	-0.920	5.025
56.264775	548.90	0.015	16.46	0	2.881	-0.069
56.363389	1344.00	1.660	11.44	0	-0.596	4.750
56.968206	1763.00	1.260	11.81	0	-0.556	4.104
57.612484	2141.00	0.915	12.21	0	-2.414	3.536
58.323877	2386.00	0.626	12.66	0	-2.635	2.686
58.446590	1457.00	0.084	14.49	0	6.848	-0.647
59.164207	2404.00	0.391	13.19	0	-6.032	1.858
59.590983	2112.00	0.212	13.60	0	8.266	-1.413
60.306061	2124.00	0.212	13.82	0	-7.170	0.916
60.434776	2461.00	0.391	12.97	0	5.664	-2.323
61.150560	2504.00	0.626	12.48	0	1.731	-3.039
61.800154	2298.00	0.915	12.07	0	1.738	-3.797
62.411215	1933.00	1.260	11.71	0	-0.048	-4.277
62.486260	1517.00	0.083	14.68	0	-4.290	0.238
62.997977	1503.00	1.665	11.39	0	0.134	-4.860
63.568518	1087.00	2.115	11.08	0	0.541	-5.079
64.127767	733.50	2.620	10.78	0	0.814	-5.525
64.678903	463.50	3.195	10.50	0	0.415	-5.520
65.224071	274.80	3.815	10.20	0	0.069	-5.520
65.764772	153.00	4.485	10.00	0	-0.143	-5.520
66.302091	80.09	5.225	9.70	0	-0.428	-5.520
66.836830	39.46	6.005	9.40	0	-0.726	-5.520
67.369598	18.32	6.845	9.20	0	-1.002	-5.520
67.900867	8.01	7.745	8.90	0	-1.255	-5.520
68.431005	3.30	8.695	8.70	0	-1.500	-5.520
68.960311	1.28	9.695	8.60	0	-1.700	-5.520
118.750343	945.00	0.009	16.30	0	-0.247	0.003
368.498350	67.90	0.049	19.20	0.6	0	0
424.763124	638.00	0.044	19.16	0.6	0	0
487.249370	235.00	0.049	19.20	0.6	0	0
715.393150	99.60	0.145	18.10	0.6	0	0
773.839675	671.00	0.130	18.10	0.6	0	0
834.145330	180.00	0.147	18.10	0.6	0	0

v0	b1	b2	b3	b4	b5	b6
22.235080	0.1090	2.143	28.11*	0.69	4.80*	1.00*
67.813960	0.0011	8.735	28.58	0.69	4.93	0.82
119.995940	0.0007	8.356	29.48	0.70	4.78	0.79
183.310074	2.3000	0.668	28.13*	0.64	5.30*	0.85*
321.225644	0.0464	6.181	23.03	0.67	4.69	0.54
325.152919	1.5400	1.540	27.83	0.68	4.85	0.74
336.187000	0.0010	9.829	26.93	0.69	4.74	0.61
380.197372	11.9000	1.048	28.73*	0.69*	5.38*	0.84*
390.134508	0.0044	7.350	21.52	0.63	4.81	0.55
437.346667	0.0637	5.050	18.45	0.60	4.23	0.48
439.150812	0.9210	3.596	21.00	0.63	4.29	0.52
443.018295	0.1940	5.050	18.60	0.60	4.23	0.50
448.001075	10.6000	1.405	26.32	0.66	4.84	0.67
470.888947	0.3300	3.599	21.52	0.66	4.57	0.65
474.689127	1.2800	2.381	23.55	0.65	4.65	0.64
488.491133	0.2530	2.853	26.02	0.69	5.04	0.72
503.568532	0.0374	6.733	16.12	0.61	3.98	0.43
504.482692	0.0125	6.733	16.12	0.61	4.01	0.45
556.936002	510.0000	0.159	32.10	0.69	4.11	1.00
620.700807	5.0900	2.200	24.38	0.71	4.68	0.68
658.006500	0.2740	7.820	32.10	0.69	4.14	1.00
752.033227	250.0000	0.396	30.60	0.68	4.09	0.84
841.073593	0.0130	8.180	15.90	0.33	5.76	0.45
859.865000	0.1330	7.989	30.60	0.68	4.09	0.84
899.407000	0.0550	7.917	29.85	0.68	4.53	0.90
902.555000	0.0380	8.432	28.65	0.70	5.10	0.95
906.205524	0.1830	5.111	24.08	0.70	4.70	0.53
916.171582	8.5600	1.442	26.70	0.70	4.78	0.78
970.315022	9.1600	1.920	25.50	0.64	4.94	0.67
987.926764	138.0000	0.258	29.85	0.68	4.55	0.90

* Measured data were chosen in favor of theoretical values

where Debye strength and width are

$$S_d = 6.14 \cdot 10^{-4} p \theta^2,$$

$$\gamma_o = 5.6 \cdot 10^{-3} (p + 1.1e) \theta,$$

and the N_2 coefficient is given by

$$a_p = 1.40(1 - 1.2 \cdot 10^{-5} f^{1.5}) 10^{-10}.$$

The width γ_o was derived from an MPM-based evaluation of zenith attenuation values, which were deduced from atmospheric noise data measured between 2.5 and 10 GHz [11].

2.3. Water-Vapor Continuum

A so-called water-vapor *continuum* N_c with the loss and delay terms [10]

$$N_c''(f) = f(b_s e + b_f p)10^{-5} e\theta^3$$
and
$$N_c'(f) = f^2 b_o(1 - 0.20\theta)10^{-5} e\theta^{2.7} \qquad (14)$$

supplements local H_2O line contributions (8), where $b_s = 3.57\theta^{7.5}$, $b_f = 0.113$, and $b_o = 0.998$.

Experimental attenuation rates α_x of moist air generally exhibit more water-vapor absorption than is contributed by the H_2O line base. The excess is most pronounced in atmospheric millimeter-wave window ranges.

Continuum absorption N_c'' was determined by a series of accurate laboratory measurements in the 140 GHz window range. Absolute attenuation $\alpha_x(P,T,U)$ was measured at f_x= 137.8 GHz for both pure water vapor and moist air under the following conditions [9]:

total pressure	P = p + e	(p = 0 to 150 kPa),
temperature	T = 8 to 43°C	(θ = 1.07 to 0.949),
rel. humidity	U = 95 %RH	(e = 0 to 0.95e_S).

The measured data could be expressed in the form

$$\alpha_x = [k_s(T)e^2 + k_f(T)ep + k_d(T)p^2]10^{-3} \quad \text{dB/km}. \qquad (15)$$

Temperature dependence of the k-coefficients was determined from fits to a power law, $k(T) = k\cdot\theta^x$, which led to

$$k_s = 133(4)\theta^{10.3(3)},$$
$$k_f = 5.68(5)\theta^{3.0(4)}, \text{ and}$$
$$k_d = .002(1)\theta^3.$$

Values in parentheses give the standard deviation from the mean in terms of the final listed digits.

Equation (15) provided benchmark data over a wide range of input variables (P,T,U) which served to *calibrate* MPM at 138 GHz. For N_c'' in (14), which gave the best fit between measured and modeled data, it was assumed that the absorption in excess of line resonance contributions is proportional to f^2.

To discuss continuum absorption at a fixed frequency, we keep the form of (14) and define

$$N''(f_x) = (c_s e\theta^y + c_f p)10^{-5} e\theta^3.$$

At f_x = 138 GHz, a quantitative evaluation of six H_2O absorption cases is summarized below:

Case	Contribution	c_s	y	c_f	Reference
1	Experiment	530	7.3	22.6	Eq.(15)
2	MPM Lines	33.4	0.5	7.0	[9]
3	MPM Continuum	493	7.5	15.6	Eq.(14)
.....					
4	Theoret. Cont.	14.4	0.5	3.03	[10]
5	Full Rot. Spectr.	109	0.5	22.6	[9]
6	EXCESS, C1 - C5	422	9.6	-	[9]

For MPM, case 1 is the sum of cases 2 + 3. Attenuation data reported from laboratory and field experiments in moist air between 10 and 430 GHz by other researchers agreed well with MPM predictions when N_c'' was included.

Case 4 resulted from a Taylor-series fit to complex refractivity N based on line-by-line calculations of the full rotational H_2O spectrum above 1 THz. The five-term imaginary part, when evaluated for Van Vleck-Weisskopf shape contributions at 138 GHz, fits the functional form of (14) but the coefficient, c_s, is much smaller than the empirical MPM continuum (see case 3). Hill's model [10] explains contributions from wings of air-broadened H_2O lines above 1 THz to be 19 percent (θ = 1) of the MPM coefficient c_f. We have experimental evidence to associate all of c_f with air broadening [9]. In case 5, we go one step further and apply the self-broadening efficiency (see b_5, TABLE 1) to yield $c_s = 4.8c_f$. This still leaves 86 percent of MPM's e^2 continuum term as excess absorption (case 6), not explained by the H_2O line spectrum.

The b_s-term of (14) with its strong negative temperature dependence, so far, has not found a sound theoretical explanation. Hypotheses about its origin consider wing contributions from self-broadened H_2O lines above 1 THz, collision-induced absorption, and water dimers - to be involved separately or collectively [2]. The results obtained are inconclusive and support neither far wing nor dimer approaches.

The real part of the continuum is insensitive to a specific shape function. Neglecting f^4 and f^6 terms, we applied the principal (f^2) term of [10] to approximate N_c'.

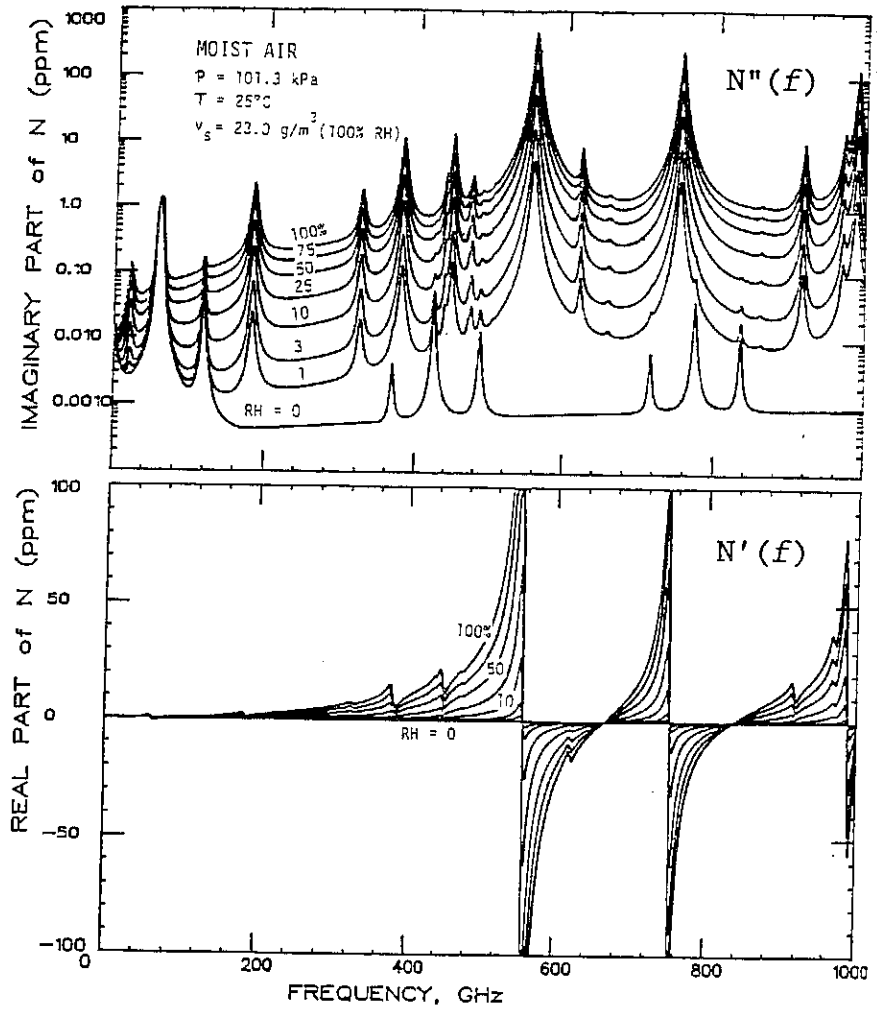

FIGURE 1. Atmospheric dispersive refractivity N = N' - jN" over the frequency range from 0 to 1000 GHz for a sea level condition (P,T) at various relative humidities (U).

Equations (8)-(14) complete the moist air part of N. The detailed structure of MPM comes best to light in a graphical presentation. Examples for a sea level condition exhibit spectra at various relative humidities (U = 0 to 100 %RH) in Figure 1. Molecular resonance absorption can be recognized in the 60 GHz band, at 119 GHz, and higher due to O_2, as well as around 22, 183 GHz, and higher due to H_2O. Across the spectrum one notices more or less transparent window ranges separated by molecular resonance peaks. Relative humidity (2) is a key variable to describe the dominating (>125 GHz) water vapor effects of absorption (*IM*) and dispersive refractivity (*RE*).

2.4. Suspended Water Droplet Refractivity

Suspended water droplets in haze, fog, or clouds are efficient millimeter-wave absorbers. Their size range of radii is below 50 μm, which allows the Rayleigh approximation of Mie scattering theory to be applied to formulate refractivity contributions N_W [12],

$$N_W''(f) = W(9/2)[\epsilon''(1+\eta^2)]^{-1},$$
and
$$N_W'(f) = W(9/2)[1/(\epsilon_o+2) - \eta/\epsilon''(1+\eta^2)], \quad (16)$$

where $\eta = (2+\epsilon')/\epsilon''$; ϵ_o is the static ($f = 0$) and ϵ', ϵ'' are the real and imaginary parts of the permittivity for liquid water. Equation (16) underestimates N_W at frequencies above 300 GHz. Mie scattering comes into play (e.g., at 1 THz, N_W'' increases by about 10 to 30 % [12]).

Dielectric permittivity $\epsilon(f)$ of water is determined with a new double-Debye model [12]:

$$\epsilon''(f) = (\epsilon_o-\epsilon_1)f/f_P[1+(f/f_P)^2] + (\epsilon_1-\epsilon_2)f/f_S[1+(f/f_S)^2],$$
and
$$\epsilon'(f) = (\epsilon_o-\epsilon_1)/[1+(f/f_P)^2] + (\epsilon_1-\epsilon_2)/[1+(f/f_S)^2] + \epsilon_2 , \quad (17)$$

where $\epsilon_o = 77.66 + 103.3(\theta-1)$,
$\epsilon_1 = 5.48$,
$\epsilon_2 = 3.51$;
and the principal and secondary relaxation frequencies are
$f_P = 20.09 - 142(\theta-1) + 294(\theta-1)^2$ GHz , and
$f_S = 590 - 1500(\theta-1)$ GHz .

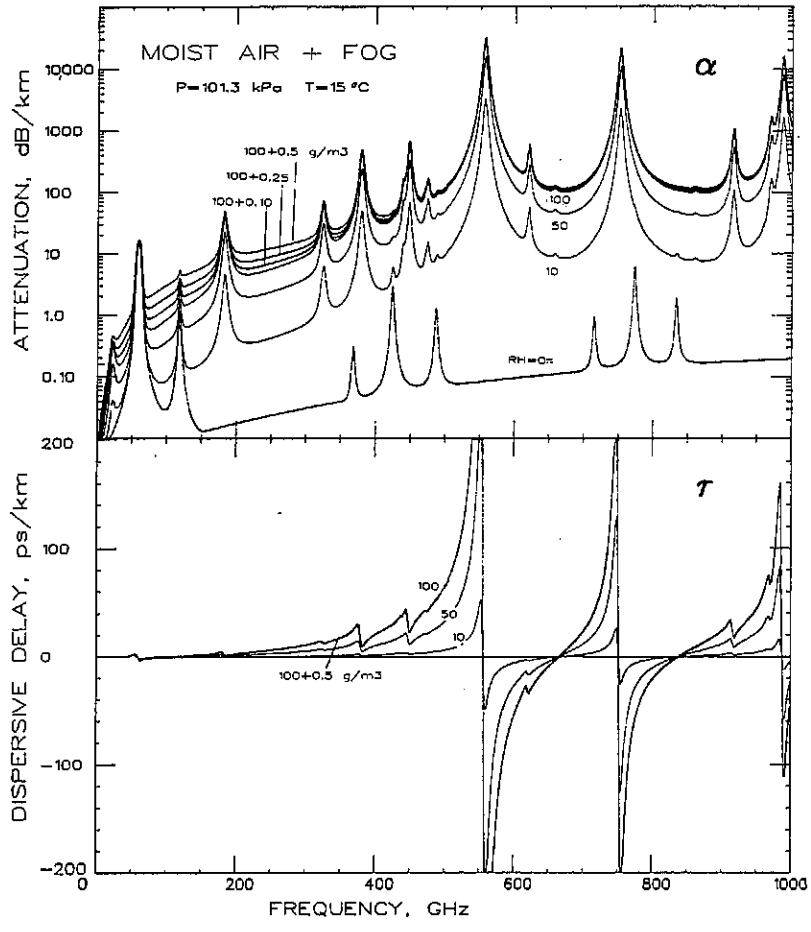

Figure 2. Attenuation (α) and delay (τ) rates for three fog cases (W = 0.1, 0.25, 0.5 g/m^3) added to a saturated sea level condition. Also shown are dry air (0 %RH) and moist air (10, 50 %RH) characteristics.

Equation (17) is a *best-fit* to permittivity data reported for frequencies up to 1000 GHz over a temperature range from -10 to 30°C.

Systems operating in the millimeter-wave (90 - 350 GHz) range offer an attractive alternative to electro-optical systems when operation has to be assured during periods of optical obscuration. Water droplet effects (16) of MPM are added to a state of saturated (U = 100 %RH) air. Key parameters are concentration W and temperature T. Typical α,τ - cases are displayed in Figure 2.

2.5. Rain Effects

Refractivity of rain, N_R, is governed by absorption and scattering effects [13]. Substantial interactions take place when drop diameters (0.1 to 5 mm) and radio wavelengths become comparable. Bypassing elaborate, lengthy Mie calculations which require drop shape and size distributions as well as the dielectric permittivity of water (17), the following approximations are used,

$$N_R''(f) \approx c_R R^z \qquad (18)$$

and

$$N_R'(f) \approx R(0.012\,R - 3.7)y^{2.5}/[f_R(1 + y^{2.5})],$$

where $y = f/f_R$ and $f_R = 53 - R(0.37 - 0.0015R)$ GHz.

Frequency dependent coefficient $c_R(f)$ and exponent $z(f)$ for the power law relation have been evaluated at T = 0°C using drop-size spectra by Laws and Parsons [14]. A regression fit to individual (c_R,z)-pairs over the frequency range from 1 to 1000 GHz resulted in the calculation scheme

$$c_R = x_1 f^{y1} \qquad \text{and} \qquad z = x_2 f^{y2},$$

where:

f	x_1	y_1	f	x_2	y_2
GHz			GHz		
1 to 2.9	$3.51\cdot10^{-4}$	1.03	1 to 8.5	0.851	0.158
2.9 to 54	$2.31\cdot10^{-4}$	1.42	8.5 to 25	1.41	-0.0779
54 to 180	0.225	-0.301	25 to 164	2.63	-0.272
180 to 1000	18.6	-1.151	164 to 1000	0.616	0.0126

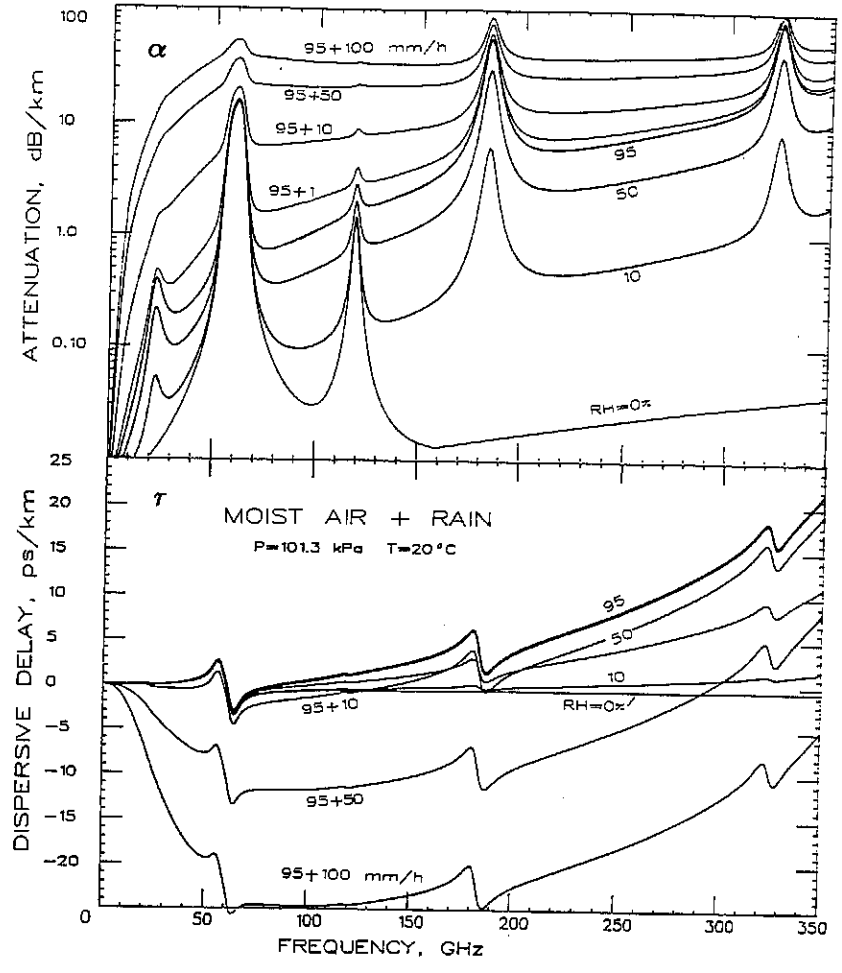

Figure 3. Attenuation (α) and delay (τ) delay rates over the frequency range from 0 to 350 GHz for four rain cases (R = 1, 10, 50, 100 mm/h) added to a sea level condition (P,T, 95 %RH). Also shown are dry (0 %RH) and moist (10, 50 %RH) air characteristics.

The formulation in (18) for refractive dispersion by rain was derived from a least-squares-fit to complex Mie calculations based on a Marshall-Palmer drop-size distribution [15].

A major concern for all systems operating at frequencies above 10 GHz is their performance in rain. The MPM rain model (18) provides estimates on propagation effects by such events (see Sect. 1.2). Predictions are made by adding to the known state of moist air (P,T,U) only one additional parameter, namely the point rainfall rate R. Examples for attenuation and delay rates of four rain cases are shown in Figure 3. Above 10 GHz, rain attenuation rates increase rapidly; actually they can be excessive above 20 GHz for a small fraction of time ($t_R < 0.01$, $R > 50$ mm/h), thus becoming a statistical problem.

3. CONCLUDING REMARKS

A parametric model of atmospheric refractivity

$$N(f;\ P,T,U;\ W;\ R)$$

was developed for applications between 1 GHz and 1 THz in areas such as telecommunications, radar, remote sensing, radio astronomy. The code MPM is organized in six modules [(6),(8),(13),(14),(16),(18)] which control over 500 parameters. A desk computer version of MPM was written to run efficiently on microcomputers (diskettes may be requested from ITS).

The MPM model given here has been updated over the version published in 1985 [1]. Validation, error checking of predictions, and incorporation of new research results will continue to be critical and time consuming tasks. Various shortcomings remain (e.g., empirical H_2O continuum absorption, oversimplified treatment of rain, omitted mesospheric O_2 Zeeman effect, missing trace gas spectra by CO, O_3, etc).

The characteristics of the water vapor spectrum in MPM are still far from being clearly understood. Especially the lack of a theoretical basis for the e^2-term of continuum absorption (14) is a source of concern. Its largely empirical origin can introduce modeling errors when predicting transmission characteristics in atmospheric window ranges. Research to uncover the true nature of the millimeter-wave water vapor continuum remains a serious challenge.

REFERENCES

[1] Liebe, H. J.: *Radio Sci.* 20 (1985) 1069.

[2] Rosenkranz, P. W.: Chapter 2 in *Atmospheric Remote Sensing By Microwave Radiometry* (M. A. Janssen, ed.), Wiley-Interscience, N.Y., 1989.

[3] Liebe, H. J., Hufford, G. H., Katz, A. S.: *Digest 13th Int. Conf. Infrared and MM Wave Conf.*, Honolulu, HI (Dec. 1988); SPIE, vol. 1039, T9.6/171.

[4] Liebe, H. J.: *Int. J. IR and MM Waves* 5 (1984) 207.

[5] Gerber, H. E.: *NRL-Report 8956*, U.S. Navy Res. Lab., Washington, DC.,December 1985.

[6] Rosenkranz, P. W.: *J. Quant. Spectr. Rad. Transf.* 39 (1988) 287.

[7] Zink, L. R., Mizushima, M.: *J. Molec. Spectr.* 125 (1987) 154.

[8] Bauer, A., Godon, M., Kheddar, M., Hartmann, J. M.: *J. Quant. Spectr. Rad. Transf.* 40 (1988) in press.

[9] Liebe, H. J., Layton, D. H.: *NTIA-Report 87-224*, U.S. Dept. Commerce, Boulder, CO., October 1987.

[10] Hill, R. J.: *IEEE Trans. Ant. Prop.*, AP-36 (1988) 423.

[11] Danese, L., Partridge, R. B.: *Astrophys. J.* 341 (1989) in press.

[12] Liebe, H. J., Manabe, T., Hufford, G. H.: *IEEE Trans. Ant. Prop.*, AP-37 (1989) in press.

[13] Oguchi, T.: *Proc. IEEE*, 71 (1983) 1029.

[14] Olsen, R. L., Rogers, D. V., Hodge, D. B.: *IEEE Trans. Ant. Prop.*, AP-26 (1978) 318.

[15] Zuffery, C. H.: MS-Thesis, Dept. Electr. Eng., University Colorado, Boulder, CO., February 1972.

International Journal of Infrared and Millimeter Waves, Vol. 10, No. 6, 1989

HIGH-GAIN FEL WITH VARIABLE PARAMETER WIGGLERS

Hui Zhong-xi

China Academy of Engineering Physics

Received February 10, 1989

ABSTRACT

A general discussion of FEL with variable parameter wigglers for the production of high power coherent radiation at reasonable efficiency is presented. Some promising modes are identified and analyzed.

INTRODUCTION

The recent successful operation of the FEL has stimulated a great deal of interest in the use of the FEL to produce a high power tunable laser beam. The maximum fractional energy that can be extracted from a constant parameter FEL is equal to 1/2N, where N is the number of wiggler periods, while the resulting energy spread of the electron beam emerging from the FEL is comparable to or greater than the mean energy loss. This places severe limitations on the overall gain, efficiency and modes of operation for the constant parameter FEL. While there are many schemes to overcome some of the limitations of the constant parameter FEL, such as the use of transverse gradients in the magnetic field of the wiggler and the coupling of the FEL with an

0195-9271/89/0600-0651$06.00/0